JACS
JOURNAL OF THE AMERICAN CHEMICAL SOCIETY
pubs.acs.org/JACS
Article

Real-Time Pyruvate Chemical Conversion Monitoring Enabled by PHIP

Gabriele Stevanato, Yonghong Ding, Salvatore Mamone, Anil P. Jagtap, Sergey Korchak, and Stefan Glöggler*

Cite This: *J. Am. Chem. Soc.* 2023, 145, 5864−5871
Read Online

ABSTRACT: In recent years, parahydrogen-induced polarization side arm hydrogenation (PHIP-SAH) has been applied to hyperpolarize [1-^{13}C]pyruvate and map its metabolic conversion to [1-^{13}C]lactate in cancer cells. Developing on our recent MINERVA pulse sequence protocol, in which we have achieved 27% [1-^{13}C]pyruvate carbon polarization, we demonstrate the hyperpolarization of [1,2-^{13}C]pyruvate (~7% polarization on each ^{13}C spin) *via* PHIP-SAH. By altering a single parameter in the pulse sequence, MINERVA enables the signal enhancement of C1 and/or C2 in [1,2-^{13}C]pyruvate with the opposite phase, which allows for the simultaneous monitoring of different chemical reactions with enhanced spectral contrast or for the same reaction *via* different carbon sites. We first demonstrate the ability to monitor the same enzymatic pyruvate to lactate conversion at 7T in an aqueous solution, *in vitro*, and in-cell (HeLa cells) *via* different carbon sites. In a second set of experiments, we use the C1 and C2 carbon positions as spectral probes for simultaneous chemical reactions: the production of acetate, carbon dioxide, bicarbonate, and carbonate by reacting [1,2-^{13}C]pyruvate with H_2O_2 at a high temperature (55 °C). Importantly, we detect and characterize the intermediate 2-hydroperoxy-2-hydroxypropanoate in real time and at high temperature.

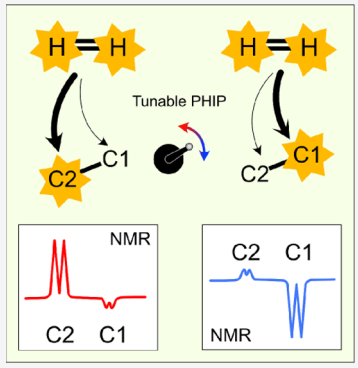

INTRODUCTION

Nuclear magnetic resonance (NMR) is a non-invasive and quantitative analytical technique with applications in structural biology,[1] drug discovery,[2] and biomedicine.[3] The limited NMR sensitivity has been tackled by hyperpolarization techniques to enhance signals over 10,000-fold with a large focus on metabolic studies. Dynamic nuclear polarization (DNP), parahydrogen-induced polarization (PHIP[4−7] and SABRE-signal amplification by reversible exchange[8−12]), and other methods have been intensively researched with this respect.[13−22] SABRE succeeded in hyperpolarizing [1-^{13}C]-acetate[23] and [1-^{13}C]pyruvate at >10% in methanol and very recently in water−methanol solution.[24−27] PHIP is relatively inexpensive and achieves carbon polarization levels similar to those of dissolution DNP on specific targets.[28] Inter alia, the PHIP side-arm hydrogenation (PHIP-SAH) method by Reineri *et al.*[29] can in principle be applied to any molecule containing a carboxylic group. In essence, a precursor molecule formed by an unsaturated moiety linked through an ester bond to the substrate of interest is hyperpolarized by PHIP, and upon hydrolysis *via* base injection (NaOH or Na_2CO_3), the hyperpolarized metabolite is retained.[29,30] The heteronuclear polarization transfer from parahydrogen is realized by magnetic field cycling (MFC) or pulsed NMR methods.[31−40]

Among the various molecular systems, pyruvate plays a crucial role in deregulated glycolytic pathways in diseases associated with inflammation, neurodegeneration, and cancer.[41,42] As the end product of glycolysis, pyruvate might be converted into alanine *via* alanine transaminase (ALT) or lactate *via* lactate dehydrogenase (LDH), or it can enter the tricarboxylic acid cycle (TCA) *via* the catalysis of the pyruvate dehydrogenase complex (PDH). The metabolic conversion of [1-^{13}C]pyruvate-to-[1-^{13}C]lactate (P−L) has shown potential in clinical trials of prostate cancer patients,[43−45] and we have recently used it to produce the first mouse tumor imaging by PHIP-SAH.[46] However, by approaching TCA, [1-^{13}C]pyruvate is converted *via* PDH into $^{13}CO_2$, thereby preventing the direct detection of downstream TCA metabolites. Instead, [2-^{13}C]-pyruvate enters TCA and can potentially be used to access, for example, [5-^{13}C]glutamate, thus broadening the range of accessible metabolic information.[47]

[1,2-^{13}C]Pyruvate combines the advantages of [1-^{13}C] and [2-^{13}C]pyruvates. It has been explored in the context of *in vitro* and *in vivo* DNP[48,49] and in that of nuclear long-lived spin states.[50,51] SABRE succeeded in [1,2-^{13}C]pyruvate ^{13}C hyperpolarization at <2% albeit in methanol-d_4.[52] In addition to its central role in cellular energy production, pyruvate plays a

Received: December 13, 2022
Published: March 1, 2023

https://doi.org/10.1021/jacs.2c13198
J. Am. Chem. Soc. 2023, 145, 5864−5871

crucial part in shielding neurons and other cell types from the harmful effects of hydrogen peroxide (H_2O_2). The primary cause of the neuroprotective effect appeared to be related to the non-enzymatic decarboxylation of α-ketoacids rather than to an improvement of energy metabolism.[53]

Here, we report on [1,2-^{13}C]pyruvate hyperpolarization *via* PHIP-SAH in combination with our maximizing insensitive nuclei enhancement reached *via* para-hydrogen amplification (MINERVA) method at 7T.[54] We control the phase and polarization levels at C1 and C2 carbon positions by only adjusting one sequence parameter: the final β pulse (see Figure 2). Hyperpolarized [1,2-^{13}C]pyruvate in an aqueous solution is used to monitor the real-time P−L conversion (Figure 1b) *in vitro* and *in-cell*. Furthermore, we show that we can track multiple chemical reactions simultaneously through the different carbon-13-tagged sites by investigating the H_2O_2-induced pyruvate decarboxylation pathway. Importantly, we report the transient real-time formation of the intermediate 2-hydroperoxy-2-hydroxypropanoate (**I**) at high temperature (55 °C) and at different pH conditions.

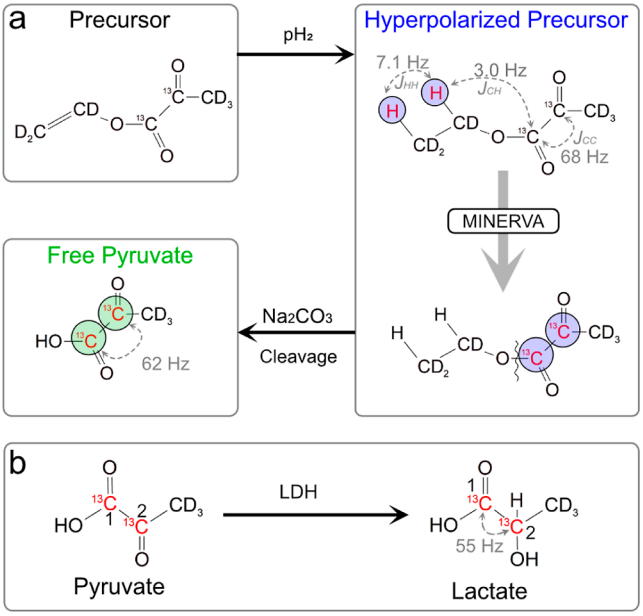

Figure 1. (a) PHIP-SAH steps: [1,2-^{13}C]perdeuterated vinyl pyruvate precursor upon parahydrogen addition converts into hyperpolarized ethyl [1,2-^{13}C]pyruvate precursor. The MINERVA sequence transfers the polarization to the $^{13}C_1$ and/or $^{13}C_2$ of the pyruvate moiety. Upon Na_2CO_3-induced hydrolysis, free [1,2-^{13}C]pyruvate is obtained. (b) Hyperpolarized (HP) P−L conversion triggered by the lactate dehydrogenase (LDH) enzyme. Circles indicate HP nuclei.

RESULTS AND DISCUSSION

PHIP-SAH. For all our studies, we used [1,2-^{13}C]-perdeuterated vinyl pyruvate which is synthesized as described in the Supporting Information[54] and used as a [1,2-^{13}C]-pyruvate PHIP-SAH precursor (see Figure 1a). Experimentally, parahydrogen at 7 bars is supplied to a degassed 100 μL acetone-d_6 solution containing 5 mM precursor and 10 mM of [1,4-Bis(diphenylphosphino)butane](1,5-cyclooctadiene)-rhodium(I) tetrafluoroborate catalyst. The duration of para-hydrogen supply was 20 s at 55 °C and 7T. The subsequent application of MINERVA transfers the parahydrogen polarization to the target carbon nuclei on the precursor molecule at C1, C2, or both positions depending on the β angle used (see below). In the following 5 s, the pressure is released, and 100 μL of a 50 mM solution of Na_2CO_3 in D_2O is injected into the NMR tube *via* a plastic cannula (i.d. 1 mm) coupled externally to a 1 mL syringe. Upon injection of the aqueous solution, the drop in catalyst's solubility initiates the catalyst's precipitation. Following the base injection, a vacuum pump connected to the NMR tube is activated for 15 s to evaporate the acetone from the acetone−D_2O mixture present in the NMR tube (see Supporting Information 3). A further 5 s delay is needed to inject 100 μL of buffer solution to adjust the aqueous pH to circumneutral values and obtain isotonicity. In the last step, a volume of 200 μL of H_2O_2, the enzymatic, or the cell solution—in different experiments—is injected through a different plastic cannula. The carbon spectrum is acquired *via* the subsequent application of 20° (45° for HeLa cell experiments) flip angle pulses every 2 s.

MINERVA. We describe the hyperpolarized precursor molecule as a four-spin system with two parahydrogen ^{1}H, I_1 and I_2, and two ^{13}C nuclear spins S_1 and S_2, with the relevant J-coupling network reported in Figure 1a. The initial state upon hydrogenation at 7T is incoherently averaged to $\rho_1 = 2\, I_{1z}I_{2z}$. The first block of the sequence (1−2 in Figure 2a) converts ρ_1 primarily into in-phase magnetization on the C1 carbon to yield $\rho_2 = S_{1y}$ which evolves through the second block (2−3 in Figure 2a) to $\rho_3 = -\cos(\beta)S_{1y} + \sin(\beta)S_{2y}$. By varying the β angle, the signal can be filtered at C1 (first block), C2 ($\beta = \pi/2$), or both carbon positions ($\beta = \pi/4$) (see Figures 2b and S8). After MINERVA ($\beta = \pi/4$) and base injection, the pyruvate chemical shifts jump from δP_1 = 162.3 ppm to δP_1 =

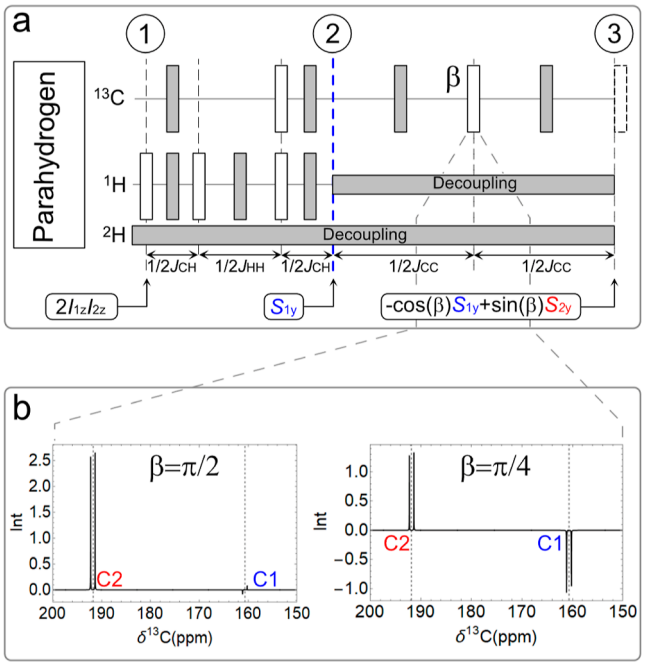

Figure 2. (a) MINERVA for the transfer of longitudinal spin order of parahydrogen into magnetization. The filled and empty rectangles are 180 and 90° pulses, respectively. The phases of the 180° pulses lay along the transverse axes of the rotating plane except for the last optional flip pulse (dashed empty rectangle) on the x-axis. The spin density operator at steps 1, 2, and 3 is reported in boxes. The last 90° dashed pulse is removed for direct observation. (b) Simulated spectra with $\beta = \pi/2$ (left) and $\beta = \pi/4$ (right).

https://doi.org/10.1021/jacs.2c13198
J. Am. Chem. Soc. 2023, 145, 5864−5871

170.5 ppm for C1 and δP_2 = 193.2 ppm to δP_2 = 205.6 ppm for C2 (see Figure 3a). Each peak is further split by J_{CC} ~ 68 Hz. The ^{13}C polarization levels (Pol) at each steps go from Pol ~ 24 ± 1.6% before cleavage to Pol ~ 7 ± 1.0% after cleavage, Pol ~ 2.5 ± 1.0% after solvent evaporation and buffer pH adjustment, to the final average Pol< ~ 1.0 ± 0.3% at the moment of H_2O_2 or enzymatic/cell solution injection (Figure 3a). The polarization levels are similar at C1 and C2. The values of T_1 at 7T and 55 °C before and after cleavage are T_1 ~ 79.5 s and T_1 ~ 63.9 s at C1 and T_1 ~ 66.7 s and T_1 ~ 45.2 s for C2. We note that based on T_1, we would expect a ~40% drop in polarization rather than ~70% after cleavage. The total volume, before solvent evaporation, of ~200 μL is still within the coil region, and no losses in signal are expected. The extreme pH before buffer adjustment can be related to the polarization loss. However, we have not tried here to investigate further this aspect. We only note that the pyruvate instantaneous polarization can also be approximately estimated *via* the asymmetry of the corresponding ^{13}C doublets as previously shown.[49,55]

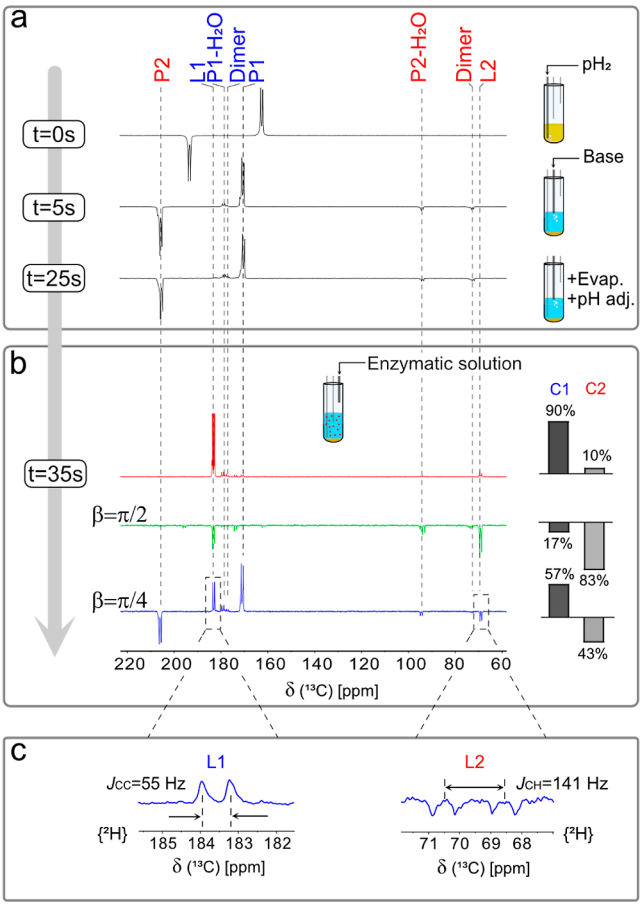

Figure 3. (a) (1) ^{13}C NMR of the precursor after hydrogenation (t = 0 s), after reaction with 50 mM Na_2CO_3 (t = 5 s), and after vacuum evaporation and pH adjustment (t = 25 s). (b) ^{13}C NMR of HP [1,2-^{13}C] P−L conversion after injection of 200 μL of 100 LDH units (t = 35 s) acquired to enhance C1 (red spectrum → only first block of MINERVA to produce S_{1y}), to enhance C2 (green spectrum → full MINERVA with $\beta = \pi/2$ to produce S_{2y}), and to enhance C1 and C2 (blue spectrum → full MINERVA with pi/4 to produce $-0.7 \times S_{1y}$ and $+0.7 \times S_{2y}$). Bar graphs indicate the fraction of the signal with C1 (positive phase) and C2 (negative phase) characteristics. (c) Expanded L_1 and L_2 regions with {^{2}H} decoupling. The vertical gray lines indicate δP_1 = 170.5 ppm (162.3 ppm before cleavage) and δP_2 = 205.6 ppm (193.2 ppm before cleavage). The hydrated forms of pyruvate, P_1-H_2O and P_2-H_2O, resonate at 179.7 and 95 ppm, respectively. Dimer forms of pyruvate at δ = 177.3 and δ = 73.0 ppm. δL_1 = 183 ppm and δL_2 = 69 ppm after injection of LDH.

***In Vitro* Enzymatic Reaction Monitoring.** In the final step, 200 μL of a buffer solution containing 100 units of rabbit muscle LDH and 20 mM NADH, thermalized at 37 °C, is injected at 7T, and the P−L conversion was monitored by 20° ^{13}C pulses every 2 s (Figure 3b). For lactate, the resonances δL_1 = 183 ppm and δL_2 = 69 ppm are observed. In Figure 3b, MINERVA is adapted to retain the signal primarily on C1 (red spectrum using the first block of the sequence, *i.e.*, 1−2 in Figure 2a), on C2 (green spectrum by $\beta = \pi/2$), and on both (blue spectrum by $\beta = \pi/4$). The expansion in Figure 3c shows the {^{2}H}^{13}C spectrum at the final step, where J_{CH} = 141 Hz splitting at 69 ppm points out L_2, whereas T_1 for P_1 and P_2 is similar (~17 s of apparent decay at 55 °C), and the T_1 ratio for L_1 and L_2 is about 3.0 (*i.e.*, ~7 s of apparent decay at 55 °C for L_2). The faster L_2 decay is partially explained by the spatial proximity of the lactate ^{1}H leading to a stronger dipolar contact. The enzymatic reaction was also monitored at 37 °C (50 LDH units). The fitting model used, introduced by Khegai and *et al.*,[56] assumes two exchanging pools with a unidirectional k_{PL}: $P \xrightarrow{k_{PL}} L$. It has been previously shown that back conversion is typically negligible[57] (see Supporting Information 5). The advantage and limitation of the model used is that the different metabolic relaxation rates are included in a single effective rate R_{eff}, and k_{PL} is obtained by a simple to compute pseudoinversion matrix operation. The table in Supporting Information 6 shows agreement between the k_{PL} values measured *via* C1 and C2 in three replicate experiments at different conditions.

In-Cell Real-Time P−L Conversion. Figure 4a shows that the P−L conversion can be followed through both carbon signatures C1 and C2, also *in-cells*. HeLa cancer cells are prepared as described in the Supporting Information. After the polarization steps detailed in Figure 3a, 200 μL of a HeLa cell slurry (~25 millions) in fresh culture medium (DMEM with supplements as per Supporting Information 3) is injected at 7T, and the ^{13}C spectrum is acquired *via* consecutive {^{1}H, ^{2}H}^{13}C 45° pulses starting approximately ~8−10 s after cell injection. In addition to the pyruvate, hydrated form, and dimer signals, the C1 and C2 signatures of lactate at 183.2 and 69.2 ppm are visible in Figure 4a,b. The experimental chemical shifts are summarized in Table 1.

The thermal spectrum in Figure 4b indicates the presence of ~5 μL residual acetone-d_6 (see Supporting Information 7). The cell viability at the end of the experiment is conservatively about >90%. Although following P−L conversion *via* MINERVA ($\beta = \pi/4$), comes at the cost of splitting the signal between C1 and C2, the combined effect of a doubly labeled pyruvate and a tunable sequence gives the highest degree of flexibility.

Factors Influencing ^{13}C Polarization. At every step in Figure 3, the polarization is affected by many parameters such as H_2 solubility, the solvent, the catalyst, and others. Acetone has a relative low toxicity[58] and guarantees a good H_2 solubility and a weak binding affinity to the Rh(I) catalyst used. This, in turn, favors an improved efficiency and better polarization levels as the fast displacement of the product molecule from the metal center limits the singlet/triplet mixing on the

https://doi.org/10.1021/jacs.2c13198
J. Am. Chem. Soc. 2023, 145, 5864−5871

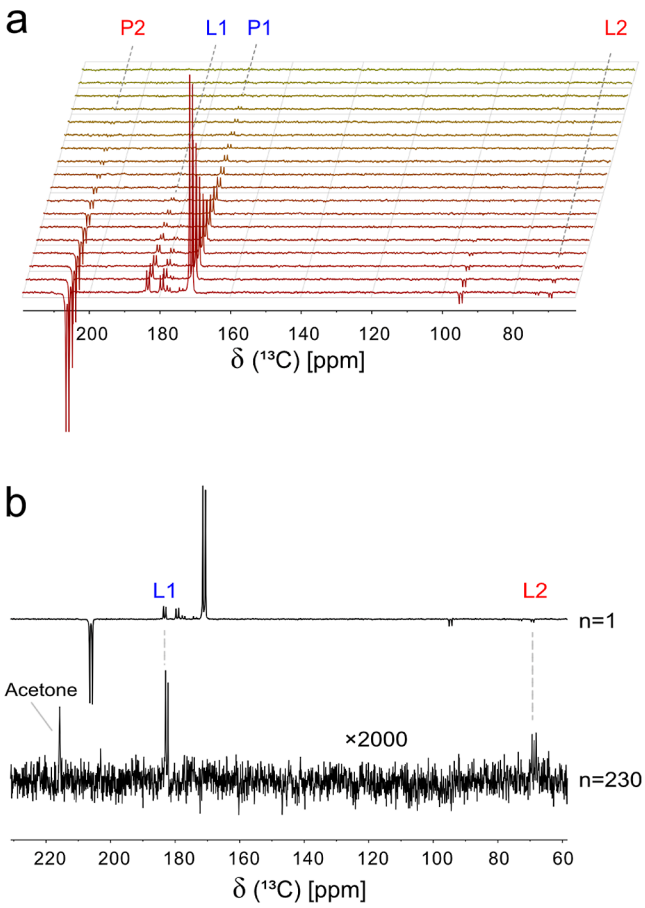

Figure 4. (a) Pseudo-2D ^{13}C NMR experiments with P−L conversion detected in HeLa cells (∼25 M) at 7T, with cells kept at 37 °C until injection. (b) ^{13}C hyperpolarized NMR spectrum (ns = 1, 45° recording angle) and thermal spectrum (ns = 230, 90°, ×2000-fold) acquired from the Hela cell sample.

Table 1. ^{13}C Chemical Shifts for the In-Cell Real-Time P−L Conversion at pH 7, T = 37 °C

	experimental chemical shifts, ppm	
	^{13}C1	^{13}C2
pyruvate	171.0	206.0
hydrate	179.3	94.6
dimer	177.3	73.0
lactate	183.2	69.2

intermediate reaction products that has been linked to loss of polarization.[59,60] We further note that for the catalyst in acetone-d_6 a turnover frequency (*i.e.*, the moles of substrate that a mole of catalyst can convert per second) higher than in other common organic solvents is observed.[60] In addition, the acetone boiling point, 58 °C, is compatible with the evaporation step we have implemented. Deuteration of the initial precursor is instrumental to polarization transfer achieved by MINERVA by restricting the effective nuclear spin system and minimizing dilution of signal enhancement. Alternative side arms are possible and were recently investigated by our group.[54] According to our studies, the precursor vinyl pyruvate granted the highest levels of carbon hyperpolarization in [1-^{13}C]pyruvate so far (*i.e.*, 59.7 ± 2.5 and 27 ± 1% on the precursor molecule and free pyruvate, respectively)[54] and was therefore the precursor of choice in the current investigation. The [1,4-Bis(diphenylphosphino)-butane](1,5-cyclooctadiene)rhodium(I) tetrafluoroborate Rh catalyst is frequently used in PHIP experiments for two main reasons: (i) it is commercially available and (ii) it enables the pairwise addition of parahydrogen, which is necessary to preserve the parahydrogen's initial spin character. In the present work, we did not attempt to compare multiple Rh catalysts. However, we note that recently it has been reported that structural modifications of the Rh catalyst used here lead to improved catalytic activity, faster hydrogenation reaction, and possibly improved ^{13}C polarization.[61]

Real-Time Pyruvate Decarboxylation Monitoring. As explained in the Introduction, pyruvate protects neurons and other cell types from the toxic hydrogen peroxide (H_2O_2).[53,62] H_2O_2 is stable in abiotic environments at ambient temperature and neutral pH, yet rapidly kills any type of cells by producing highly reactive hydroxyl radicals. Although catalases are commonly deployed by cells as powerful H_2O_2 scavengers,[63] pyruvate is also used to quench H_2O_2 by reacting quickly and irreversibly to yield acetate and carbon dioxide. According to a proposed mechanism, supported by experimental results with $H_2{}^{18}O_2$, the product formation in the H_2O_2-induced pyruvate decarboxylation occurs through the intermediate 2-hydroxyperoxy-2-hydroxypropanoate (**I**)[64−66] (see Figure 5a). Low-temperature ^{13}C NMR and UV spectrophotometry have been used to capture **I**'s presence.[64,65] However, the real-time monitoring of **I** at high temperature by NMR has been hampered so far by the low sensitivity and limited lifetime. In Figure 5b, we report the stacked plot showing the ^{13}C NMR for the non-enzymatic decarboxylation of [1,2-^{13}C]pyruvate according to the reaction in Figure 5a. The experiment has been conducted at 55 °C following the steps already described in Figure 3a. In short, we applied MINERVA to hyperpolarize 5 mM [1,2-^{13}C]pyruvate as per Figure 1a. After injecting the buffer solution to bring the pH to 7 (pH 2 and 9 in other experiments, see Supporting Information 6.1), we waited 4 s before applying a series of 20-degree flip angle pulses to track the ^{13}C NMR signal. The ^{13}C NMR spectra at the bottom of Figure 5b,c show the presence of pyruvate, the corresponding hydrated form, and the dimer signals.[65] In the final step, after the injection of 200 μL of H_2O_2 at 326 mM (H_2O_2 1%), the ^{13}C NMR spectrum drastically changes. The middle spectrum in Figure 5c shows a negative and a positive signal both separated into two peaks 64 Hz apart (squared dashed box). The spectral positions are compatible with the previously reported values for **I** in methanol/water in ref 65. These signals are relatively short-lived as they vanish 12 s after the H_2O_2 injection, as shown in the top transient (20 s) in Figure 5c. We attribute these two signals to the C1 and C2 signatures of [1,2-^{13}C]**I** due to their opposite phases, identical 64 Hz splitting, short lifetime, and compatibility with previously reported values.[65] In addition to the [1,2-^{13}C]**I** formation, we observe the presence of all of the species detailed in Figure 5a−c, whose chemical shift is reported in Table 2 for clarity. The carbon polarization is sufficiently high to investigate the formation of acetate and CO_2 in a single experiment using the intermediate [1,2-^{13}C]**I** and the C2 and C1 carbon signatures of [1,2-^{13}C]pyruvate, respectively. Conveniently, the positive and negative NMR signals correspond to the carbon spins at C1 and C2, respectively. Therefore, different carbon sites are useful for investigating different simultaneous chemical processes.

https://doi.org/10.1021/jacs.2c13198
J. Am. Chem. Soc. 2023, 145, 5864−5871

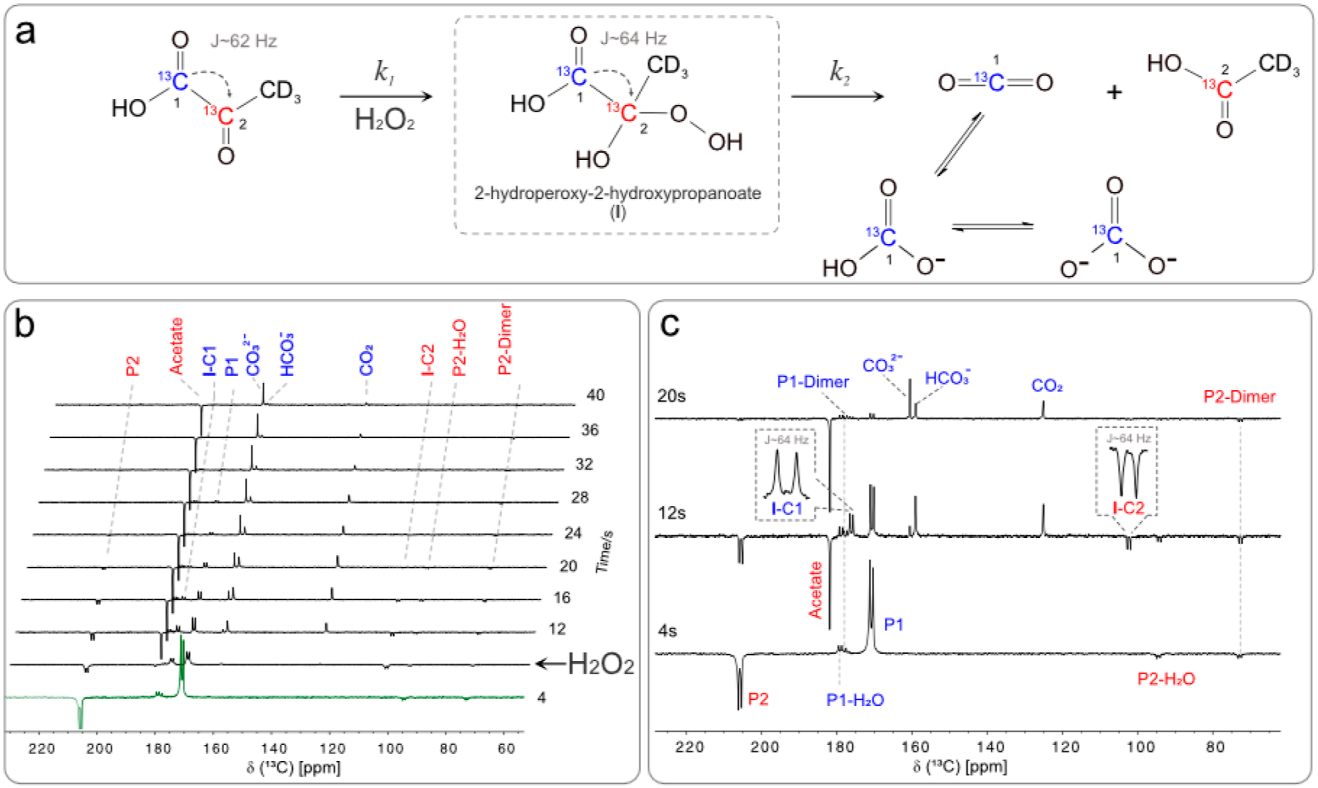

Figure 5. (a) Non-enzymatic decarboxylation reaction between [1,2-^{13}C]pyruvate (5 mM) and H_2O_2 (326 mM) *via* the intermediate formation of 2-hydroxyperoxy-2-hydroxypropanoate (**I**) at pH 7. The C1 and C2 ^{13}C positions are indicated in blue and red, respectively. (b) Series of ^{13}C hyperpolarized NMR spectra (20-degree flip angle). The green spectrum at 4s shows hyperpolarized [1,2-^{13}C]pyruvate. From 8s, after the injection of H_2O_2, the spectra report on the H_2O_2-induced [1,2-^{13}C]pyruvate decarboxylation reaction. Species deriving from C1 and C2 are indicated vertically in blue and red, respectively. (c) 1D ^{13}C NMR extracts from the pseudo 2D experiment in (b) before (bottom) and after (middle and top) the injection of H_2O_2. Evidence of **I** at 12 s *via* C1 and C2 positions at 176.1 and 102.3 ppm with J_{C1C2} ~ 64 Hz. Pyruvate has almost completely been consumed by the reaction in the top spectrum with loss of spectral signature for **I**.

Table 2. ^{13}C Chemical Shifts for the Various Species in the Pyruvate Decarboxylation Reaction at pH 7, T = 55 °C

	experimental chemical shifts, ppm	
	^{13}C1	^{13}C2
pyruvate	170.6	205.6
hydrate	178.8	94.4
dimer	177.6	72.6
intermediate (**I**)	176.1	102.3
acetate		181.4
bicarbonate	159.0	
carbonate	160.5	
carbon dioxide	125.0	

By using the pathway in Figure 5a as a guide, a fitting model for the reaction rates k_1 and k_2 was developed. The model (see Supporting Information 6) is oversimplified because (i) we omit the pyruvate equilibria of its hydrate and dimer forms as they have the weakest signal in our spectra; (ii) we treat carbon dioxide, bicarbonate, and carbonate as a single product since the equilibria among them is irrelevant for the intermediate formation; and (iii) we assume unidirectional reaction rates. From the analysis detailed in the Supporting Information, assuming a T_1 = 50 s for pyruvate (the same at C1 and C2, as per conventional NMR under similar conditions), T_1 = 3.0 s for **I** (the same at C1 and C2, as different values seem to be less compatible with our experimental data), we find that k_1 = 0.18 s^{-1} and k_2 = 0.23 s^{-1} with a T_1 = 25 s for acetate at 7T. Furthermore, the signals from CO_2 and HCO_3^- in Figure 5b have similar lifetimes, and as can be seen in Figure 5c, they show comparable polarization levels at each transient. Under these premises and taking into account the fast exchange regime between CO_2 and HCO_3^-, a stable pH is found throughout the chemical reaction by taking the integral ratio of HCO_3^- and CO_2 according to the Henderson−Hasselbalch equation (eq. Supporting Information 9) at each transient (Figure S15). Additional experiments were conducted at pH = 2 and pH = 9 (see Supporting Information 6.1). At pH = 2 in particular, we see that HCO_3^- forms from $^{13}CO_2$ as the bicarbonate at ~159 ppm signature is only visible after carbon dioxide formation at ~123 ppm (carbon signals in the dashed gray box in Figure S14b). At basic conditions (pH = 9), pyruvate is immediately quenched by reacting with H_2O_2, and we neither observe the formation of **I** nor of $^{13}CO_2$ (Figure S14a).

■ CONCLUSIONS

In conclusion, we succeeded in hyperpolarizing [1,2-^{13}C]-pyruvate *via* PHIP-SAH. We investigated the P−L metabolic conversion kinetics in aqueous solution *in vitro* and *in-cells* at 7T. To the best of our knowledge, although previous reports on doubly labeled pyruvate hyperpolarization exist,[48,50,52] no measure of the kinetics *via* C1, C2, or both was reported so far by PHIP-SAH-based techniques.

We also follow in real-time the non-enzymatic pyruvate decarboxylation through different carbon sites C1 and C2,

https://doi.org/10.1021/jacs.2c13198
J. Am. Chem. Soc. 2023, 145, 5864−5871

confirming the intermediate formation of 2-hydroperoxy-2-hydroxypropanoate (**I**) that was previously reported only by low-temperature ^{13}C NMR and not in real time.

In the proposed experiment, the pH of the solution can be monitored in real time by tracking the production of $H^{13}CO_3^-$ and $^{13}CO_2$ during the decarboxylation reaction *via* the correspondent carbon signals.

We think that the possibility to follow various chemical reactions or the same reaction *via* different carbon sites, as we show here, without the need of numerous metabolic probes *via* a straightforward and widely accessible PHIP-SAH protocol is particularly noteworthy. The NMR pulse strategy used is flexible and allows for the selective or simultaneous hyperpolarization of C1 and C2 with opposite phase by only changing a single pulse in the MINERVA sequence. We show that the kinetics information can be extracted for P−L conversion from either C1 or C2 site. This approach may also be of use to better analyze mixtures of metabolites that are tagged with different phases in the same sample.

■ ASSOCIATED CONTENT

Supporting Information

The Supporting Information is available free of charge at https://pubs.acs.org/doi/10.1021/jacs.2c13198.

Chemical synthesis, enzyme and cell experiments, hyperpolarization experiments, kinetic fitting, and simulations (PDF)

■ AUTHOR INFORMATION

Corresponding Author

Stefan Glöggler − *NMR Signal Enhancement Group, Max Planck Institute for Multidisciplinary Sciences, 37077 Göttingen, Germany; Center for Biostructural Imaging of Neurodegeneration of the University Medical Center Göttingen, 37075 Göttingen, Germany;* orcid.org/0000-0003-3354-6141; Email: stefan.gloeggler@mpinat.mpg.de

Authors

Gabriele Stevanato − *NMR Signal Enhancement Group, Max Planck Institute for Multidisciplinary Sciences, 37077 Göttingen, Germany; Center for Biostructural Imaging of Neurodegeneration of the University Medical Center Göttingen, 37075 Göttingen, Germany*

Yonghong Ding − *NMR Signal Enhancement Group, Max Planck Institute for Multidisciplinary Sciences, 37077 Göttingen, Germany; Center for Biostructural Imaging of Neurodegeneration of the University Medical Center Göttingen, 37075 Göttingen, Germany*

Salvatore Mamone − *NMR Signal Enhancement Group, Max Planck Institute for Multidisciplinary Sciences, 37077 Göttingen, Germany; Center for Biostructural Imaging of Neurodegeneration of the University Medical Center Göttingen, 37075 Göttingen, Germany*

Anil P. Jagtap − *NMR Signal Enhancement Group, Max Planck Institute for Multidisciplinary Sciences, 37077 Göttingen, Germany; Center for Biostructural Imaging of Neurodegeneration of the University Medical Center Göttingen, 37075 Göttingen, Germany*

Sergey Korchak − *NMR Signal Enhancement Group, Max Planck Institute for Multidisciplinary Sciences, 37077 Göttingen, Germany; Center for Biostructural Imaging of Neurodegeneration of the University Medical Center Göttingen, 37075 Göttingen, Germany*

Complete contact information is available at: https://pubs.acs.org/10.1021/jacs.2c13198

Funding

The authors thank the Max Planck Society for generous funding. This project received funding from the Deutsche Forschungsgemeinschaft (DFG) (Grants 418416679, 426677227, and 450146057) and the European Research Council (ERC) under the European Union's Horizon 2020 research and innovation program (Grant Agreement 949180). Open access funded by Max Planck Society.

Notes

The authors declare no competing financial interest.

■ ABBREVIATIONS

MFC	magnetic field cycling
PHIP	parahydrogen-induced polarization
SABRE	signal amplification by reversible exchange
MINERVA	maximizing insensitive nuclei enhancement reached *via* para-hydrogen amplification
P−L	pyruvate to lactate

■ REFERENCES

(1) Theillet, F. X. In-Cell Structural Biology by NMR: The Benefits of the Atomic Scale. *Chem. Rev.* **2022**, *122*, 9497−9570.

(2) Pellecchia, M.; Sem, D. S.; Wüthrich, K. NMR in drug discovery. *Nat. Rev. Drug Discov.* **2002**, *1*, 211−219.

(3) Hövener, J. B.; Pravdivtsev, A. N.; Kidd, B.; Bowers, C. R.; Glöggler, S.; Kovtunov, K. V.; Plaumann, M.; Katz-Brull, R.; Buckenmaier, K.; Jerschow, A.; Reineri, F.; Theis, T.; Shchepin, R. V.; Wagner, S.; Bhattacharya, P.; Zacharias, N. M.; Chekmenev, E. Y. Parahydrogen-Based Hyperpolarization for Biomedicine. *Angew. Chem., Int. Ed. Engl.* **2018**, *57*, 11140−11162.

(4) Bowers, C. R.; Weitekamp, D. P. Transformation of symmetrization order to nuclear-spin magnetization by chemical reaction and nuclear magnetic resonance. *Phys. Rev. Lett.* **1986**, *57*, 2645−2648.

(5) Bowers, C. R.; Weitekamp, D. P. Parahydrogen and synthesis allow dramatically enhanced nuclear alignment. *J. Am. Chem. Soc.* **1987**, *109*, 5541−5542.

(6) Chekmenev, E. Y.; Norton, V. A.; Weitekamp, D. P.; Bhattacharya, P. Hyperpolarized 1H NMR Employing Low γ Nucleus for Spin Polarization Storage. *J. Am. Chem. Soc.* **2009**, *131*, 3164−3165.

(7) Kaltschnee, L.; Jagtap, A. P.; McCormick, J.; Wagner, S.; Bouchard, L. S.; Utz, M.; Griesinger, C.; Glöggler, S. Hyperpolarization of Amino Acids in Water Utilizing Parahydrogen on a Rhodium Nanocatalyst. *Chemistry* **2019**, *25*, 11031−11035.

(8) Adams, R. W.; Aguilar, J. A.; Atkinson, K. D.; Cowley, M. J.; Elliott, P. I.; Duckett, S. B.; Green, G. G.; Khazal, I. G.; López-Serrano, J.; Williamson, D. C. Reversible interactions with para-hydrogen enhance NMR sensitivity by polarization transfer. *Science* **2009**, *323*, 1708−1711.

(9) Rayner, P. J.; Burns, M. J.; Olaru, A. M.; Norcott, P.; Fekete, M.; Green, G. G. R.; Highton, L. A. R.; Mewis, R. E.; Duckett, S. B. Delivering strong 1H nuclear hyperpolarization levels and long magnetic lifetimes through signal amplification by reversible exchange. *Proc. Natl. Acad. Sci. U.S.A.* **2017**, *114*, E3188−E3194.

(10) Barskiy, D. A.; Kovtunov, K. V.; Koptyug, I. V.; He, P.; Groome, K. A.; Best, Q. A.; Shi, F.; Goodson, B. M.; Shchepin, R. V.; Coffey, A. M.; Waddell, K. W.; Chekmenev, E. Y. The Feasibility of Formation and Kinetics of NMR Signal Amplification by Reversible Exchange (SABRE) at High Magnetic Field (9.4 T). *J. Am. Chem. Soc.* **2014**, *136*, 3322−3325.

(11) Theis, T.; Truong, M. L.; Coffey, A. M.; Shchepin, R. V.; Waddell, K. W.; Shi, F.; Goodson, B. M.; Warren, W. S.; Chekmenev, E. Y. Microtesla SABRE enables 10% nitrogen-15 nuclear spin polarization. *J. Am. Chem. Soc.* **2015**, *137*, 1404−1407.
(12) Truong, M. L.; Shi, F.; He, P.; Yuan, B. X.; Plunkett, K. N.; Coffey, A. M.; Shchepin, R. V.; Barskiy, D. A.; Kovtunov, K. V.; Koptyug, I. V.; Waddell, K. W.; Goodson, B. M.; Chekmenev, E. Y. Irreversible Catalyst Activation Enables Hyperpolarization and Water Solubility for NMR Signal Amplification by Reversible Exchange. *J. Phys. Chem. B* **2014**, *118*, 13882−13889.
(13) Walker, T. G.; Happer, W. Spin-exchange optical pumping of noble-gas nuclei. *Rev. Mod. Phys.* **1997**, *69*, 629−642.
(14) King, J. P.; Jeong, K.; Vassiliou, C. C.; Shin, C. S.; Page, R. H.; Avalos, C. E.; Wang, H. J.; Pines, A. Room-temperature in situ nuclear spin hyperpolarization from optically pumped nitrogen vacancy centres in diamond. *Nat. Commun.* **2015**, *6*, 8965.
(15) Kuhn, L. T. Photo-CIDNP NMR spectroscopy of amino acids and proteins. *Top. Curr. Chem.* **2013**, *338*, 229−300.
(16) Matysik, J.; Ding, Y. H.; Kim, Y.; Kurle, P.; Yurkovskaya, A.; Ivanov, K.; Alia, A. Photo-CIDNP in Solid State. *Appl. Magn. Reson.* **2021**, *53*, 521−537.
(17) Eichhorn, T. R.; Parker, A. J.; Josten, F.; Müller, C.; Scheuer, J.; Steiner, J. M.; Gierse, M.; Handwerker, J.; Keim, M.; Lucas, S.; Qureshi, M. U.; Marshall, A.; Salhov, A.; Quan, Y.; Binder, J.; Jahnke, K. D.; Neumann, P.; Knecht, S.; Blanchard, J. W.; Plenio, M. B.; Jelezko, F.; Emsley, L.; Vassiliou, C. C.; Hautle, P.; Schwartz, I. Hyperpolarized Solution-State NMR Spectroscopy with Optically Polarized Crystals. *J. Am. Chem. Soc.* **2022**, *144*, 2511−2519.
(18) Liu, G.; Levien, M.; Karschin, N.; Parigi, G.; Luchinat, C.; Bennati, M. One-thousand-fold enhancement of high field liquid nuclear magnetic resonance signals at room temperature. *Nat. Chem.* **2017**, *9*, 676−680.
(19) Orlando, T.; Dervişoğlu, R.; Levien, M.; Tkach, I.; Prisner, T. F.; Andreas, L. B.; Denysenkov, V. P.; Bennati, M. Dynamic Nuclear Polarization of 13 C Nuclei in the Liquid State over a 10 Tesla Field Range. *Angew. Chem., Int. Ed. Engl.* **2019**, *58*, 1402−1406.
(20) Elliott, S. J.; Stern, Q.; Ceillier, M.; El Daraï, T.; Cousin, S. F.; Cala, O.; Jannin, S. Practical dissolution dynamic nuclear polarization. *Prog. Nucl. Magn. Reson. Spectrosc.* **2021**, *126−127*, 59−100.
(21) Ardenkjaer-Larsen, J. H.; Fridlund, B.; Gram, A.; Hansson, G.; Hansson, L.; Lerche, M. H.; Servin, R.; Thaning, M.; Golman, K. Increase in signal-to-noise ratio of > 10,000 times in liquid-state NMR. *Proc. Natl. Acad. Sci. U.S.A.* **2003**, *100*, 10158−10163.
(22) Golman, K.; Ardenkjær-Larsen, J. H.; Petersson, J. S.; Månsson, S.; Leunbach, I. Molecular imaging with endogenous substances. *Proc. Natl. Acad. Sci. U.S.A.* **2003**, *100*, 10435−10439.
(23) Gemeinhardt, M. E.; Limbach, M. N.; Gebhardt, T. R.; Eriksson, C. W.; Eriksson, S. L.; Lindale, J. R.; Goodson, E. A.; Warren, W. S.; Chekmenev, E. Y.; Goodson, B. M. "Direct"13C Hyperpolarization of13C-Acetate by MicroTesla NMR Signal Amplification by Reversible Exchange (SABRE). *Angew. Chem., Int. Ed. Engl.* **2020**, *59*, 418−423.
(24) TomHon, P.; Abdulmojeed, M.; Adelabu, I.; Nantogma, S.; Kabir, M. S. H.; Lehmkuhl, S.; Chekmenev, E. Y.; Theis, T. Temperature Cycling Enables Efficient 13C SABRE-SHEATH Hyperpolarization and Imaging of [1-13C]-Pyruvate. *J. Am. Chem. Soc.* **2022**, *144*, 282−287.
(25) Adelabu, I.; TomHon, P.; Kabir, M. S. H.; Nantogma, S.; Abdulmojeed, M.; Mandzhieva, I.; Ettedgui, J.; Swenson, R. E.; Krishna, M. C.; Theis, T.; Goodson, B. M.; Chekmenev, E. Y. Order-Unity 13C Nuclear Polarization of [1-13C]Pyruvate in Seconds and the Interplay of Water and SABRE Enhancement. *ChemPhysChem* **2022**, *23*, No. e202100839.
(26) Chapman, B.; Joalland, B.; Meersman, C.; Ettedgui, J.; Swenson, R. E.; Krishna, M. C.; Nikolaou, P.; Kovtunov, K. V.; Salnikov, O. G.; Koptyug, I. V.; Gemeinhardt, M. E.; Goodson, B. M.; Shchepin, R. V.; Chekmenev, E. Y. Low-Cost High-Pressure Clinical-Scale 50% Parahydrogen Generator Using Liquid Nitrogen at 77 K. *Anal. Chem.* **2021**, *93*, 8476−8483.
(27) Schmidt, A. B.; de Maissin, H.; Adelabu, I.; Nantogma, S.; Ettedgui, J.; TomHon, P.; Goodson, B. M.; Theis, T.; Chekmenev, E. Y. Catalyst-Free Aqueous Hyperpolarized [1-13C]Pyruvate Obtained by Re-Dissolution Signal Amplification by Reversible Exchange. *ACS Sens.* **2022**, *7*, 3430−3439.
(28) Korchak, S.; Mamone, S.; Glöggler, S. Over 50 % 1 H and 13 C Polarization for Generating Hyperpolarized Metabolites—A para -Hydrogen Approach. *ChemistryOpen* **2018**, *7*, 672−676.
(29) Reineri, F.; Boi, T.; Aime, S. ParaHydrogen Induced Polarization of 13C carboxylate resonance in acetate and pyruvate. *Nat. Commun.* **2015**, *6*, 5858.
(30) Jóhannesson, H.; Axelsson, O.; Karlsson, M. Transfer of para-hydrogen spin order into polarization by diabatic field cycling. *Compt. Rendus Phys.* **2004**, *5*, 315−324.
(31) Goldman, M.; Jóhannesson, H.; Axelsson, O.; Karlsson, M. Hyperpolarization of 13C through order transfer from parahydrogen: A new contrast agent for MRI. *Magn. Reson. Imag.* **2005**, *23*, 153−157.
(32) Kadlecek, S.; Emami, K.; Ishii, M.; Rizi, R. Optimal transfer of spin-order between a singlet nuclear pair and a heteronucleus. *J. Magn. Reson.* **2010**, *205*, 9−13.
(33) Dagys, L.; Jagtap, A. P.; Korchak, S.; Mamone, S.; Saul, P.; Levitt, M. H.; Glöggler, S. Nuclear hyperpolarization of (1-13C)-pyruvate in aqueous solution by proton-relayed side-arm hydrogenation. *Analyst* **2021**, *146*, 1772−1778.
(34) Stevanato, G. Alternating Delays Achieve Polarization Transfer (ADAPT) to heteronuclei in PHIP experiments. *J. Magn. Reson.* **2017**, *274*, 148−162.
(35) Stevanato, G.; Eills, J.; Bengs, C.; Pileio, G. A pulse sequence for singlet to heteronuclear magnetization transfer: S2hM. *J. Magn. Reson.* **2017**, *277*, 169−178.
(36) Korchak, S.; Yang, S.; Mamone, S.; Glöggler, S. Pulsed Magnetic Resonance to Signal-Enhance Metabolites within Seconds by utilizing para -Hydrogen. *ChemistryOpen* **2018**, *7*, 344−348.
(37) Haake, M.; Natterer, J.; Bargon, J. Efficient NMR pulse sequences to transfer the parahydrogen-induced polarization to hetero nuclei. *J. Am. Chem. Soc.* **1996**, *118*, 8688−8691.
(38) Korchak, S.; Jagtap, A. P.; Glöggler, S. Signal-enhanced real-time magnetic resonance of enzymatic reactions at millitesla fields. *Chem. Sci.* **2020**, *12*, 314−319.
(39) Korchak, S.; Emondts, M.; Mamone, S.; Blümich, B.; Glöggler, S. Production of highly concentrated and hyperpolarized metabolites within seconds in high and low magnetic fields. *Phys. Chem. Chem. Phys.* **2019**, *21*, 22849−22856.
(40) Mamone, S.; Jagtap, A. P.; Korchak, S.; Ding, Y.; Sternkopf, S.; Glöggler, S. A Field-Independent Method for the Rapid Generation of Hyperpolarized [1-13C]Pyruvate in Clean Water Solutions for Biomedical Applications. *Angew. Chem., Int. Ed.* **2022**, *61*, No. e202206298.
(41) Day, S. E.; Kettunen, M. I.; Gallagher, F. A.; Hu, D. E.; Lerche, M.; Wolber, J.; Golman, K.; Ardenkjaer-Larsen, J. H.; Brindle, K. M. Detecting tumor response to treatment using hyperpolarized 13C magnetic resonance imaging and spectroscopy. *Nat. Med.* **2007**, *13*, 1382−1387.
(42) Kurhanewicz, J.; Vigneron, D. B.; Brindle, K.; Chekmenev, E. Y.; Comment, A.; Cunningham, C. H.; DeBerardinis, R. J.; Green, G. G.; Leach, M. O.; Rajan, S. S.; Rizi, R. R.; Ross, B. D.; Warren, W. S.; Malloy, C. R. Analysis of cancer metabolism by imaging hyperpolarized nuclei: prospects for translation to clinical research. *Neoplasia* **2011**, *13*, 81−97.
(43) Nelson, S. J.; Kurhanewicz, J.; Vigneron, D. B.; Larson, P. E. Z.; Harzstark, A. L.; Ferrone, M.; van Criekinge, M.; Chang, J. W.; Bok, R.; Park, I.; Reed, G.; Carvajal, L.; Small, E. J.; Munster, P.; Weinberg, V. K.; Ardenkjaer-Larsen, J. H.; Chen, A. P.; Hurd, R. E.; Odegardstuen, L. I.; Robb, F. J.; Tropp, J.; Murray, J. A. Metabolic imaging of patients with prostate cancer using hyperpolarized [1-13C]pyruvate. *Sci. Transl. Med.* **2013**, *5*, 198ra108.
(44) de Kouchkovsky, I.; Chen, H. Y.; Ohliger, M. A.; Wang, Z. J.; Bok, R. A.; Gordon, J. W.; Larson, P. E. Z.; Frost, M.; Okamoto, K.; Cooperberg, M. R.; Kurhanewicz, J.; Vigneron, D. B.; Aggarwal, R.

https://doi.org/10.1021/jacs.2c13198
J. Am. Chem. Soc. 2023, 145, 5864−5871

Hyperpolarized 1-[13C]-Pyruvate Magnetic Resonance Imaging Detects an Early Metabolic Response to Immune Checkpoint Inhibitor Therapy in Prostate Cancer. *Eur. Urol.* **2022**, *81*, 219−221.
(45) Kurhanewicz, J.; Vigneron, D. B.; Ardenkjaer-Larsen, J. H.; Bankson, J. A.; Brindle, K.; Cunningham, C. H.; Gallagher, F. A.; Keshari, K. R.; Kjaer, A.; Laustsen, C.; Mankoff, D. A.; Merritt, M. E.; Nelson, S. J.; Pauly, J. M.; Lee, P.; Ronen, S.; Tyler, D. J.; Rajan, S. S.; Spielman, D. M.; Wald, L.; Zhang, X. L.; Malloy, C. R.; Rizi, R. Hyperpolarized 13C MRI: Path to Clinical Translation in Oncology. *Neoplasia* **2019**, *21*, 1−16.
(46) Hune, T.; Mamone, S.; Schroeder, H.; Jagtap, A. P.; Sternkopf, S.; Stevanato, G.; Korchak, S.; Fokken, C.; Müller, C. A.; Schmidt, A. B.; Becker, D.; Glöggler, S. Metabolic Tumor Imaging with Rapidly Signal-Enhanced 1-13C-Pyruvate-d3. *ChemPhysChem* **2023**, *24*, No. e202200615.
(47) Hu, S.; Yoshihara, H. A.; Bok, R.; Zhou, J.; Zhu, M.; Kurhanewicz, J.; Vigneron, D. B. Use of hyperpolarized [1-13C]pyruvate and [2-13C]pyruvate to probe the effects of the anticancer agent dichloroacetate on mitochondrial metabolism in vivo in the normal rat. *Magn. Reson. Imag.* **2012**, *30*, 1367−1372.
(48) Chen, A. P.; Hurd, R. E.; Schroeder, M. A.; Lau, A. Z.; Gu, Y. P.; Lam, W. W.; Barry, J.; Tropp, J.; Cunningham, C. H. Simultaneous investigation of cardiac pyruvate dehydrogenase flux, Krebs cycle metabolism and pH, using hyperpolarized [1,2-13C2]pyruvatein vivo. *NMR Biomed.* **2012**, *25*, 305−311.
(49) Lau, J. Y.; Chen, A. P.; Gu, Y. P.; Cunningham, C. H. A calibration-based approach to real-timein vivomonitoring of pyruvate C1and C2polarization using theJCCspectral asymmetry. *NMR Biomed.* **2013**, *26*, 1233−1241.
(50) Marco-Rius, I.; Tayler, M. C.; Kettunen, M. I.; Larkin, T. J.; Timm, K. N.; Serrao, E. M.; Rodrigues, T. B.; Pileio, G.; Ardenkjaer-Larsen, J. H.; Levitt, M. H.; Brindle, K. M. Hyperpolarized singlet lifetimes of pyruvate in human blood and in the mouse. *NMR Biomed.* **2013**, *26*, 1696−1704.
(51) Mandzhieva, I.; Adelabu, I.; Chekmenev, E. Y.; Theis, T. Proton-Only Sensing of Hyperpolarized [1,2-13C2]Pyruvate. *ACS Sens.* **2022**, *7*, 3773−3781.
(52) Iali, W.; Roy, S. S.; Tickner, B. J.; Ahwal, F.; Kennerley, A. J.; Duckett, S. B. Hyperpolarising Pyruvate through Signal Amplification by Reversible Exchange (SABRE). *Angew. Chem., Int. Ed. Engl.* **2019**, *58*, 10271−10275.
(53) Desagher, S.; Glowinski, J.; Prémont, J. Pyruvate protects neurons against hydrogen peroxide-induced toxicity. *J. Neurosci.* **1997**, *17*, 9060−9067.
(54) Ding, Y.; Korchak, S.; Mamone, S.; Jagtap, A. P.; Stevanato, G.; Sternkopf, S.; Moll, D.; Schroeder, H.; Becker, S.; Fischer, A.; Gerhardt, E.; Outeiro, T. F.; Opazo, F.; Griesinger, C.; Glöggler, S. Rapidly Signal-enhanced Metabolites for Atomic Scale Monitoring of Living Cells with Magnetic Resonance. *Chem. Methods* **2022**, *2*, No. e202200023.
(55) Datta, K.; Spielman, D. M. Doublet asymmetry for estimating polarization in hyperpolarized 13 C-pyruvate studies. *NMR Biomed.* **2017**, *30*, No. e3670.
(56) Khegai, O.; Schulte, R. F.; Janich, M. A.; Menzel, M. I.; Farrell, E.; Otto, A. M.; Ardenkjaer-Larsen, J. H.; Glaser, S. J.; Haase, A.; Schwaiger, M.; Wiesinger, F. Apparent rate constant mapping using hyperpolarized [1-13C]pyruvate. *NMR Biomed.* **2014**, *27*, 1256−1265.
(57) Cavallari, E.; Carrera, C.; Aime, S.; Reineri, F. Metabolic Studies of Tumor Cells Using [1-13 C] Pyruvate Hyperpolarized by Means of PHIP-Side Arm Hydrogenation. *Chemphyschem* **2019**, *20*, 318−325.
(58) U.S. Department of Health and Human Services, Public Health Service, Agency for Toxic Substances and Disease Registry. Toxicological Profile for Acetone. Last revised June 2022, https://www.atsdr.cdc.gov/toxprofiles/tp21.pdf (accessed Feb 16, 2023).
(59) Berner, S.; Schmidt, A. B.; Zimmermann, M.; Pravdivtsev, A. N.; Glöggler, S.; Hennig, J.; von Elverfeldt, D.; Hövener, J. B. SAMBADENA Hyperpolarization of 13 C-Succinate in an MRI: Singlet-Triplet Mixing Causes Polarization Loss. *Chemistryopen* **2019**, *8*, 728−736.
(60) Bondar, O.; Cavallari, E.; Carrera, C.; Aime, S.; Reineri, F. Effect of the hydrogenation solvent in the PHIP-SAH hyperpolarization of [1-13C]pyruvate. *Catal. Today* **2022**, *397−399*, 94−102.
(61) Itoda, M.; Naganawa, Y.; Ito, M.; Nonaka, H.; Sando, S. Structural exploration of rhodium catalysts and their kinetic studies for efficient parahydrogen-induced polarization by side arm hydrogenation. *RSC Adv.* **2019**, *9*, 18183−18190.
(62) Shostak, A.; Gotloib, L.; Kushnier, R.; Wajsbrot, V. Protective Effect of Pyruvate upon Cultured Mesothelial Cells Exposed to 2 mM Hydrogen Peroxide. *Nephron* **2000**, *84*, 362−366.
(63) Mahaseth, T.; Kuzminov, A. Potentiation of hydrogen peroxide toxicity: From catalase inhibition to stable DNA-iron complexes. *Mutat. Res. Rev. Mutat. Res.* **2017**, *773*, 274−281.
(64) Lopalco, A.; Dalwadi, G.; Niu, S.; Schowen, R. L.; Douglas, J.; Stella, V. J. Mechanism of Decarboxylation of Pyruvic Acid in the Presence of Hydrogen Peroxide. *J. Pharm. Sci.* **2016**, *105*, 705−713.
(65) Asmus, C.; Mozziconacci, O.; Schöneich, C. Low-Temperature NMR Characterization of Reaction of Sodium Pyruvate with Hydrogen Peroxide. *J. Phys. Chem. A* **2015**, *119*, 966−977.
(66) Melzer, E.; Schmidt, H. L. Carbon isotope effects on the decarboxylation of carboxylic acids. Comparison of the lactate oxidase reaction and the degradation of pyruvate by H2O2. *Biochem. J.* **1988**, *252*, 913−915.

https://doi.org/10.1021/jacs.2c13198
J. Am. Chem. Soc. 2023, 145, 5864−5871